

# NN-Copula-CD: A Copula-Guided Interpretable Neural Network for Change Detection in Heterogeneous Remote Sensing Images

Weiming Li, Xueqian Wang, and Gang Li\*

*Department of Electronic Engineering, Tsinghua University, Beijing 100084, China*

## Abstract

Change detection (CD) in heterogeneous remote sensing images is a practical and challenging issue for real-life emergencies. In the past decade, the heterogeneous CD problem has significantly benefited from the development of deep neural networks (DNN). However, the data-driven DNNs always perform like a black box where the lack of interpretability limits the trustworthiness and controllability of DNNs in most practical CD applications. As a strong knowledge-driven tool to measure correlation between random variables, Copula theory has been introduced into CD, yet it suffers from non-robust CD performance without manual prior selection for Copula functions. To address the above issues, we propose a knowledge-data-driven heterogeneous CD method (NN-Copula-CD) based on the Copula-guided interpretable neural network. In our NN-Copula-CD, the mathematical characteristics of Copula are designed as the losses to supervise a simple fully connected neural network to learn the correlation between bi-temporal image patches, and then the changed regions are identified via binary classification for the correlation coefficients of all image patch pairs of the bi-temporal images. We conduct in-depth experiments on three datasets with multimodal images (e.g., Optical, SAR, and NIR), where the quantitative results and visualized analysis demonstrate both the effectiveness and interpretability of the proposed NN-Copula-CD.

**Keywords:** Change detection (CD), heterogeneous remote sensing image, neural network, Copula.

---

\* Corresponding author: Gang Li (Email: gangli@tsinghua.edu.cn)

# I. Introduction

Change detection (CD) is a practical and crucial technology applied in many earth observation tasks, including disaster monitoring [1, 2], land-use management [3], and ecosystem protection [4]. The aim of CD is to monitor natural and man-made changes by comparing the remote sensing images with the same geographical location acquired at different times. Depending on the modalities of remote sensing images involved in CD, CD can be categorized into homogenous CD and heterogeneous CD. The homogeneous CD relies on remote sensing images with the same modality (i.e., captured by the same kind of sensors), and has been extensively investigated for the past decades. In recent years, with the proliferation of satellites and the rapid development of various imaging sensors, the availability of heterogeneous remote sensing images (i.e., captured by the different kinds of sensors) has significantly increased and even surpasses that of homogenous remote sensing images. Furthermore, the complementarity between heterogeneous data can provide better resilience against the interference of different imaging conditions (e.g., illumination and atmospheric environments) compared to homogeneous data. Overall, the heterogeneous CD has demonstrated its great potential and superiority in many applications, especially for time-sensitive emergencies such as natural disasters, and has been attracting more and more attention from scholars and practitioners alike.

Due to the heterogeneity in remote sensing images shot by different sensors, the direct pixel comparison using algebraic calculation [5-7] for homogeneous CD is not feasible. To solve this issue, one intuitive idea [8, 9] is to classify the heterogeneous images separately in the same category space, and then the decision-level fusion is performed based on the classification results of each temporal to recognize the location of changes. Note that the divide-and-conquer treatment in [8, 9] for multimodal images suppresses the impact of the heterogeneity to a certain extent, yet its performance heavily relies on the precision of the classification algorithms used for each modal. Moreover, the assumption of the same category spaces in pre/post-change images may be unattainable in many practical scenes.

Another natural insight for heterogeneous CD is to transform the bi-temporal images into the same feature space where they are easier to be compared. Following this insight, earlier works [10, 11] exploited the 3-D information of the land objects and the imaging parameters of the satellites to predict the characteristics of pre-change land objects in the post-change

assuming no event occurred. Then, the similarity between the predicted characteristics and real characteristics of land objects in the post-change scenes is calculated to identify whether the change happens. Since the 3-D information and satellite parameters are difficult to acquire in most cases, later works [12, 13] estimated the homogeneous transformation functions directly from remote sensing images via the  $K$ -nearest neighbors algorithm. Note that the machine-learning-based methods [12, 13] achieve superior performance than [10, 11] while the heavy computational cost of them and requirements for high-quality training samples still limit their usability [1].

Recently, with the rapid advancement and powerful representation capabilities of deep learning technologies, many impressive methods based on DNNs for heterogeneous CD are continuously emerging. Refs. [1] and [14] exploited deep convolution networks with a symmetric structure to transform heterogeneous images into a common feature space and extract the bi-temporal features with consistent representations. Refs. [15] and [16] employed a deep image style transfer network to convert heterogeneous image pairs into a homogeneous style space, preserving the semantic contents of each image while transforming the texture information into a uniform style. In [17-19], the generative adversarial networks (GAN) are utilized to translate one image into the domain of the other image, where the heterogeneity between images of different modalities noticeably decreases and the saliency of changes is enhanced. Furthermore, the autoencoders in [20] and [21] align the features of two heterogeneous images in a latent space via adversarial training to facilitate the learning of the image-to-image translation functions. It is worth mentioning that the above DNN-based methods have made significant progress for heterogeneous CD, however, the operating mechanisms and internal principles of DNNs are incomprehensible and invisible to us in most cases. The main reason for this is that most existing DNN-based heterogeneous CD methods suffer from the deficiencies of theoretical interpretability, leading to the degraded trustworthiness and controllability in practical applications.

Copula theory is an effective tool to model correlation between random variables. It describes the joint distribution function of random variables via a Copula function and their respective marginal distribution functions, thereby separating the randomness and coupling of random variables. In fact, the CD problem can be also transformed into a correlation measurement issue since the correlations between remote sensing region pairs at the changed

location and the unchanged location are explicitly different. In [22] and [23], the Copula theory is applied to capture the correlation between bi-temporal heterogeneous images in unchanged areas, and quantile regression according to the obtained correlation is carried out to calculate the local statistics of the post-change image assuming there is no change happening. Note that the Copula functions used in [22] and [23] are manually selected from the existing Copula families via empirical estimation of the joint distribution of two images. In practice, the joint distribution of heterogeneous image pairs varies much with different scenarios, sensors, etc. Thus, selecting the most suitable Copula function from the existing Copula families for various scenes is labor-consuming. Besides, most existing Copula functions are customized for other fields such as finance while few are for remote sensing field, which also hinders the usability of Copula theory in remote sensing applications.

In recent years, some studies [24-26] have attempted to utilize neural networks to approximate the Copula function. Thanks to the powerful representation capabilities of neural networks, Copula functions learned by neural networks exhibit a similar or even superior generalization than the traditional Copula functions. Inspired by the insights [24] of the generative Copula, we propose a novel semi-supervised method based on the Copula-guided neural network for heterogeneous CD, named NN-Copula-CD, to improve the interpretability of the existing DNN-based heterogeneous CD methods while extending the robustness and usability of the Copulas applied for remote sensing data. In the proposed NN-Copula-CD, we first segment the bi-temporal images into image patches and choose an unchanged region for training. Then, a fully connected neural network is trained under the guidance of Copula theory to learn the “unchanged correlation” between the bi-temporal image patch pairs involved in the training region. Next, the trained Copula model is exploited to estimate the “unchanged correlation” coefficients for all image patch pairs in bi-temporal images, where the “unchanged correlation” coefficients are high/low at the unchanged/changed regions, respectively. Finally, the fuzzy c-means algorithm is utilized to classify all image patch pairs into the changed and unchanged categories according to the estimated “unchanged correlation” coefficients. In summary, the main contributions of our work are as follows:

- A new knowledge-data-driven method (NN-Copula-CD) based on the Copula-guided neural network is proposed for heterogeneous CD. In NN-Copula-CD, we train a simple fully connected neural network under the guidance of Copula theory, and exploit it to



estimate the correlation between the pre-change and post-change image patches to identify the changed regions. During this process, the generalization capabilities of data-driven neural networks are integrated with the theoretical basis of knowledge-driven Copulas, which significantly improves the interpretability and robustness of the existing DNN-based and Copula-based heterogeneous CD methods, respectively.

- The experimental results on three heterogeneous CD datasets demonstrate the superiority of the proposed NN-Copula-CD over the commonly used methods on kappa coefficient and percentage correct classification. The visualized analysis exhibits the effectiveness and interpretability of our method.

The rest of this paper is organized as follows. Section II reviews the Copula theory and the existing heterogeneous CD methods based on neural networks. Section III delineates the formulations and specifics of the proposed NN-Copula-CD. Section IV presents the in-depth experiments and discussion on three heterogeneous CD datasets. Finally, the conclusion is drawn in Section IV.

## II. Related Works

### A. Copula Function

The Copula function is a strong statistical tool to analyze the dependence between random variables. Sklar's theorem indicates that the joint distribution of multivariate random variables can be represented in terms of the marginal distribution of each random variable and a Copula function. The Copula function separates the inter-correlation of random variables from their complex original distribution after transforming their original distribution into marginal probability functions that are all uniformly distributed on  $[0,1]$ . Generally speaking, the Copula function allows one to analyze the dependence between random variables and the distribution of each random variable separately, which provides a convenient and effective way to deal with complex correlation problems in quantitative finance, signal processing, healthy management, etc.

Exploiting the traditional Copula functions for CD is not an innovative concept. Mercier *et al.* [23] propose a regression model based on conditional Copula that generates the simulated post-event statistics from the observation samples of pre-event statistics, where the simulated post-event statistics and the real post-event statistics are then compared via the Kullback-

Leibler divergence to identify the changes. Note that the Copula function used in [23] needs to be specified manually, however, since most Copula functions are custom-made for finance and other fields, it is difficult to find a generalized Copula function to robustly fit the remote sensing data of different scenarios. Thus, the CD performance could be seriously degraded once we choose an inappropriate Copula function.

### *B. Neural Networks in Heterogeneous Change Detection*

In the past decades, neural networks have become a hot topic for the CD problem due to their powerful nonlinear modeling capabilities. Regarding the heterogeneous CD issue, various neural networks (e.g., image-to-image translation networks, image style transfer networks, and deep homogeneous transformation networks) have been utilized to address the challenge of heterogeneity.

For the image-to-image translation networks [17-20], Niu *et al.* [19] employed the conditional generative adversarial network (cGAN) to translate one image into the representation space of the other image, and then directly compared the translated source image and the original target image to obtain the CD results. Later Refs. [18] and [20] extended Niu's work [19] by improving cGAN with the idea of cycle-consistent adversarial networks (CycleGANs) that provides superior stability and translation performance. Additionally, translation errors are also considered in [18], where a random forest classifier replaces the original direct comparison to improve the robustness of detection results.

For the image style transfer networks, Refs. [15, 16] leverage the different layers of the VGG network to extract the semantic features and the style features separately, and then transfer the style features into the homogeneous space while preserving the semantic features unchanged. Then, the changed areas can be easily recognized via a homogeneous CD method.

For the deep homogeneous transformation networks, the coupling network in [14] simultaneously transforms the bi-temporal heterogeneous images into the homogeneous feature space in deep coupling convolution layers, where the extracted deep homogeneous features can be directly compared to identify the changes. Furthermore, a Siamese network proposed in [1] focuses on the deep-level feature transformation where the efficiency of the deep homogeneous transformation network has been significantly improved.

Note that although the neural networks in the current heterogeneous CD methods [1, 14-20]

have delivered an outstanding performance, their lack of interpretability remains a significant issue. This deficiency results in limited trustworthiness and controllability since the operating mechanism of most existing networks for heterogeneous CD is like a black box for researchers. Therefore, in this paper, we attempt to improve the interpretability of the neural networks for heterogeneous CD via the theoretical guidance of Copula.

### III. Proposed NN-Copula-CD Method

In this section, we first formulate the issue of heterogeneous CD and show the overall framework of the proposed method. Then, the steps of superpixel segmentation and feature extraction are provided. Next, we delineate the implementation details of the Copula-guided interpretable neural network. Last, we introduce the generation approach for the CD results.

#### A. Problem Formulation and Method Overview

Assume that  $I^{T_1} \in R^{H \times W \times C_{T_1}}$  and  $I^{T_2} \in R^{H \times W \times C_{T_2}}$  are bi-temporal heterogeneous remote sensing images shot in the same location at the pre-event time  $T_1$  and after-event time  $T_2$ , respectively. The goal of CD is to recognize the change events between  $I^{T_1}$  and  $I^{T_2}$  while producing a pixel-level binary result to indicate the changed areas. Note that the height  $H$  and width  $W$  of  $I^{T_1}$  and  $I^{T_2}$  should be same while the band  $C_{T_1}$  and  $C_{T_2}$  of  $I^{T_1}$  and  $I^{T_2}$  could be different.

The core idea of our method is that we first construct the “unchanged correlation” between the unchanged regions at the pre-event and after-event time, which is implemented by training a neural Copula function with a few manually selecting unchanged image patch pairs. After training over, we obtain a Copula function that reflects the unchanged tendency of input image patch pairs. Next, we can test the trained Copula model on the whole bi-temporal images, where the unchanged image patch pairs tend to be strongly correlated and the changed image patch pairs tend to be weakly correlated. Based on the correlation coefficients provided by the trained Copula function, we can efficiently identify where have changes via some commonly used clustering algorithms.

The overall framework of the proposed method is shown in Fig. 1. Our method is based on the semi-supervised mechanism, and the training process can be divided into four steps (red

stream in Fig. 1), i.e., superpixel segmentation, training sample selection, feature extraction, and neural Copula model training. After obtaining the trained neural Copula model, we test the whole image pair to produce the CD result via the trained model. The test process also consists of four steps (blue stream in Fig. 1.), i.e., superpixel segmentation, feature extraction, neural Copula model inferring, and clustering segmentation.

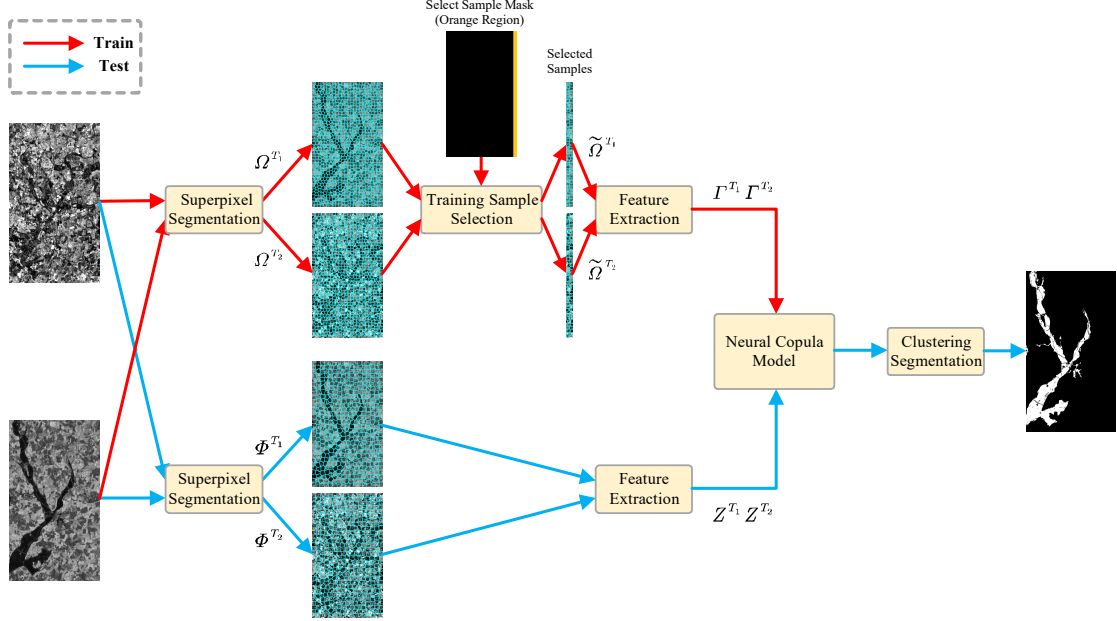


Fig. 1. The overall framework of the proposed NN-Copula-CD.

### B. Superpixel Segmentation and Training Sample Selection

It is a common situation that the size of remote sensing images is much larger than natural images. In addition, heterogeneity caused by different sensors and registration errors also seriously challenge the dependence analysis on pixel level. Therefore, it is not efficient and robust to directly build the pixel-to-pixel correlation from heterogeneous remote sensing images. In the proposed method, we choose the superpixel as the basic analysis target. Here, we introduce a collaborative simple linear iterative clustering (SLIC) algorithm [27] that is also used in [28] to segment heterogeneous image pairs into superpixel pairs. The SLIC algorithm is originally proposed for optical images with RGB channels so it struggles to deal with multi-modal remote sensing images in heterogeneous CD. To tackle this issue, the researchers in [28] propose a modified Co-SLIC algorithm, which customizes the color distance calculation rules for images with different modalities and achieves the co-segmentation for bi-temporal images. In our implementation, we also follow this modified

$\overline{SLIC}(\cdot)$  algorithm [28] to perform superpixel segmentation. The process of superpixel segmentation can be formulated as:

$$\begin{aligned}\Omega^{T_1}, \Omega^{T_2} &= \overline{SLIC}(I^{T_1}, I^{T_2}, N_1), \\ \Omega^{T_1} &= \{\Omega_i^{T_1} | i = 1, 2, \dots, N_1\}, \\ \Omega^{T_2} &= \{\Omega_i^{T_2} | i = 1, 2, \dots, N_1\},\end{aligned}\tag{1}$$

where  $\Omega^{T_1}$  and  $\Omega^{T_2}$  are superpixel sets of  $I^{T_1}$  and  $I^{T_2}$  after segmentation with parameter  $N_1$ , and  $N_1$  is manually specified parameter that controls the num of superpixel to be segmented.  $\Omega^{T_1}$  and  $\Omega^{T_2}$  are the  $i$ -th superpixel that is the set represented by the corresponding pixels of  $I^{T_1}$  and  $I^{T_2}$ , respectively. Note that  $\Omega^{T_1}$  and  $\Omega^{T_2}$  are corresponding superpixel that contains the pixels of the same position in original  $I^{T_1}$  and  $I^{T_2}$ , respectively.

Once the superpixel segmentation is completed, we choose a few unchanged superpixel pairs as training samples to fit the neural Copula function. Note that it is time-consuming and labor-intensive to check whether the superpixels are suitable as training samples one by one. Thus, we prefer to delimit a regular training region (e.g., rectangular region) in advance, as shown in Fig. 1}. Those superpixel pairs used for training will be picked from  $\Omega^{T_1}$  and  $\Omega^{T_2}$  by the principle that whether the intersection over union (IOU) between the superpixel and the selected regular region is larger than 0.5. Suppose that  $\Lambda^{T_1}$  and  $\Lambda^{T_2}$  are the pixel sets from  $I^{T_1}$  and  $I^{T_2}$  corresponding to the position of the regular training region, the process of training sample selection is formally expressed as:

$$\begin{aligned}\tilde{\Omega}^{T_1} &= \{\Omega_j^{T_1} | \frac{Num(\Omega_j^{T_1} \cap \Lambda^{T_1})}{Num(\Omega_j^{T_1})} > 0.5, \Omega_j^{T_1} \in \Omega^{T_1}, 1 \leq j \leq N_1\}, \\ \tilde{\Omega}^{T_2} &= \{\Omega_j^{T_2} | \frac{Num(\Omega_j^{T_2} \cap \Lambda^{T_2})}{Num(\Omega_j^{T_2})} > 0.5, \Omega_j^{T_2} \in \Omega^{T_2}, 1 \leq j \leq N_1\},\end{aligned}\tag{2}$$

where  $Num(\cdot)$  is the function that counts the number of elements in the set.  $\tilde{\Omega}^{T_1} \in \mathbb{R}^{N_2 \times 1}$  and  $\tilde{\Omega}^{T_2} \in \mathbb{R}^{N_2 \times 1}$  are the training superpixel set selected by checking the first to the last superpixel in  $\Omega^{T_1}$  and  $\Omega^{T_2}$  with formula (2), respectively.

Next, we need to extract the features of each selected training superpixel. Here, we directly exploit the mean value of all pixels within each training superpixel as the feature of the one. Formally,

$$\begin{aligned}I^{T_1} &= \{\gamma_k^{T_1} = Floor(Mean(\tilde{\Omega}_k^{T_1})), 1 \leq k \leq N_2\}, \\ I^{T_2} &= \{\gamma_k^{T_2} = Floor(Mean(\tilde{\Omega}_k^{T_2})), 1 \leq k \leq N_2\},\end{aligned}\tag{3}$$

where  $Mean(\cdot)$  is the function calculating the mean value of all the pixels in the corresponding superpixel.  $\Gamma^{T_1}$  and  $\Gamma^{T_2}$  are the sets containing the mean value of each training superpixel in  $\tilde{\Omega}^{T_1}$  and  $\tilde{\Omega}^{T_2}$ , respectively.

### C. Neural Copula Model

The design of traditional Copula functions is knowledge-driven, which means that people already know the prior information of the data distribution and a certain Copula function will pay more attention to fitting the correlation of the distribution of its interest. However, the prior information of the distribution of remote sensing data is difficult to estimate, thus, we always have no idea which Copula function is the most approximate before data is certain and may waste a lot of time to find the best one. To address this issue, we adopt a new neural Copula model in [24] to learn the correction directly from remote sensing data.

The first step of Copula theory is to carry the probability integral transformation (PIT) for each marginal distribution, i.e., estimating the CDF values for every point in  $\Gamma^{T_1}$  and  $\Gamma^{T_2}$ . In our implementation, we exploit kernel density estimation (KDE) [29] to estimate the CDF values for every point  $\gamma_k^{T_1}$  and  $\gamma_k^{T_2}$  in  $\Gamma^{T_1}$  and  $\Gamma^{T_2}$ , respectively. Suppose that  $KDE(X, Y)$  denotes that estimating the CDF values at every point in  $Y$  according to the distribution fitted by samples in  $X$ . The estimation for CDF values in  $\Gamma^{T_1}$  and  $\Gamma^{T_2}$  can be formulated as:

$$\begin{aligned}\tilde{\mathbf{u}} &= KDE(\Gamma^{T_1}, \Gamma^{T_1}), \\ \tilde{\mathbf{v}} &= KDE(\Gamma^{T_2}, \Gamma^{T_2}),\end{aligned}\tag{4}$$

where  $\tilde{\mathbf{u}}$  and  $\tilde{\mathbf{v}}$  are the CDF values estimated from  $\Gamma^{T_1}$  and  $\Gamma^{T_2}$ , respectively. However, it is very slow to estimate the CDF value for a large number of points directly using the KDE algorithm, we adopt the lookup-table operation to speed up the process of CDF estimation. Since the pixel value only ranges from 0 to 255 in most remote sensing images, we only need to estimate the CDF values at pixel value of 0~255 to form the CDF value tables of the distributions of  $\Gamma^{T_1}$  and  $\Gamma^{T_2}$ . Then, we can obtain the CDF values at all points in  $\Gamma^{T_1}$  and  $\Gamma^{T_2}$  by lookup-table operation.

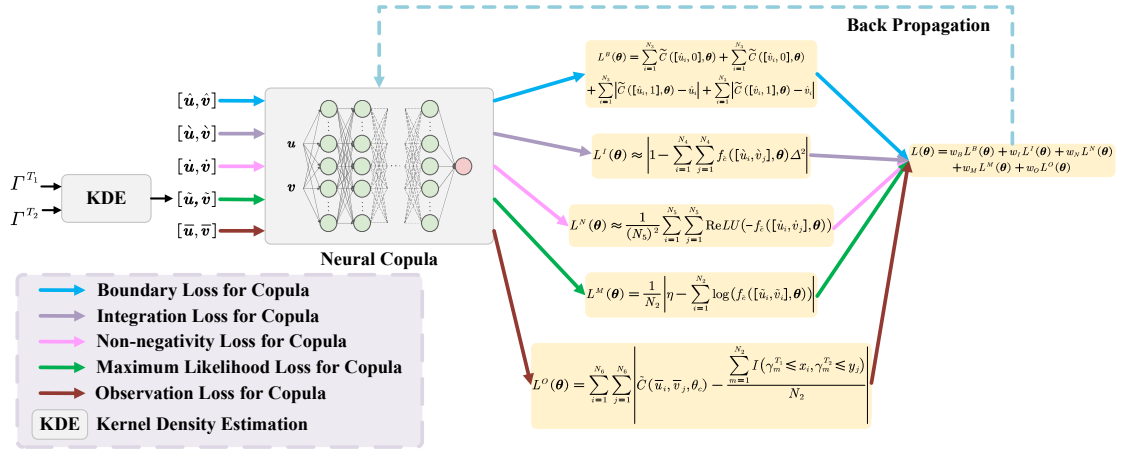


Fig. 2. The training diagram of the neural Copula.

Next, we introduce the network structure and the training process of the neural Copula. As shown in Fig. 2, the neural Copula model is a simple fully connected neural network including three parts, i.e., input layer, hidden layer, and output layer. In our experiment, we design a fully connected neural network with five hidden layers and twenty neurons per layer as the neural Copula model. Suppose that the network is written as  $\tilde{C}([\cdot], \theta)$  and  $\theta$  is the trainable parameters. The input CDF values are  $[u, v] \in \mathbb{R}^{N \times 2}$  where  $u \in \mathbb{R}^{N \times 1}$  and  $v \in \mathbb{R}^{N \times 1}$  are the vectors containing  $N$  CDF values of marginal distribution  $U$  and  $V$ , respectively. The output  $\tilde{C}([u, v], \theta)$  of the network is CDF values of the trained Copula function while the gradient  $f_{\tilde{C}}([u, v], \theta)$  of the networks is probability density function (PDF) values of the trained Copula function. To prevent PDF of neural Copula from being negative, we need to conduct non-negative processing for the gradient  $f_{\tilde{C}}([u, v], \theta)$  of the networks. Formally,

$$f_{\tilde{C}}([u, v], \theta) = \frac{\tilde{C}([u, v], \theta)}{\partial u \partial v}, \quad (5)$$

$$\bar{f}_{\tilde{C}}([u, v], \theta) = \text{ReLU}(f_{\tilde{C}}([u, v], \theta)) + \rho,$$

where  $\text{ReLU}(\cdot)$  is rectified linear unit function [30], and  $\rho$  is a minuscule positive value that is set to 1e-9 in our experiments.

Afterward, we will show how we tap the potential of this simple neural network and train it efficiently under the guidance of Copula theory. During the training process, we push the fully connected neural network to converge into the form of a Copula function via five mathematical losses.

### 1) Boundary Constraint for Neural Copula

The distribution of  $\tilde{C}([\cdot], \theta)$  should obey the boundary constraint of Copula's definition, i.e.,

$$\begin{cases} \tilde{C}([\hat{\mathbf{u}}, 0], \theta) = 0 \\ \tilde{C}([0, \hat{\mathbf{v}}], \theta) = 0 \\ \tilde{C}([\hat{\mathbf{u}}, 1], \theta) = \hat{\mathbf{u}} \\ \tilde{C}([1, \hat{\mathbf{v}}], \theta) = \hat{\mathbf{v}} \end{cases}, \quad \hat{\mathbf{u}} = [\hat{u}_1, \hat{u}_2, \dots, \hat{u}_{N_3}] \in [0, 1]^{N_3}, \quad \hat{\mathbf{v}} = [\hat{v}_1, \hat{v}_2, \dots, \hat{v}_{N_3}] \in [0, 1]^{N_3}, \quad (6)$$

where  $\hat{\mathbf{u}}$  and  $\hat{\mathbf{v}}$  are two linearly spaced vectors with  $N_3$  points generated between 0 and 1. The  $[\hat{\mathbf{u}}, 0]$ ,  $[0, \hat{\mathbf{v}}]$ ,  $[\hat{\mathbf{u}}, 1]$ , and  $[1, \hat{\mathbf{v}}]$  are the boundary point sets of the Copula function. Thus, the boundary loss for neural Copula can be defined as:

$$\begin{aligned} L^B(\theta) = & \sum_{i=1}^{N_3} \tilde{C}([\hat{u}_i, 0], \theta) + \sum_{i=1}^{N_3} \tilde{C}([0, \hat{v}_i], \theta) \\ & + \sum_{i=1}^{N_3} |\tilde{C}([\hat{u}_i, 1], \theta) - \hat{u}_i| + \sum_{i=1}^{N_3} |\tilde{C}([1, \hat{v}_i], \theta) - \hat{v}_i|, \end{aligned} \quad (7)$$

### 2) Integration Constraint for Neural Copula

The integration of PDF of all points on the domain of the Copula function should be 1. When PDF is continuous, the integration loss can be formulated as:

$$L^I(\theta) = \left| 1 - \int_{u_i \in \mathbf{u}} \int_{v_j \in \mathbf{v}} \bar{f}_c([u_i, v_j], \theta) du_i dv_j \right|, \quad (8)$$

However, we couldn't sample continuous PDF in practice. Thus, we need to rewrite the formula (8) in its approximate form. Suppose that  $\hat{\mathbf{u}} = [\hat{u}_1, \hat{u}_2, \dots, \hat{u}_{N_4}]$  and  $\hat{\mathbf{v}} = [\hat{v}_1, \hat{v}_2, \dots, \hat{v}_{N_4}]$  are both linearly spaced vectors with  $N_4$  points generated between 0 and 1.  $\Delta$  is the linear step width and equals to  $1/(N_4 - 1)^2$ , the integration loss in the discrete case can be approximated as:

$$L^I(\theta) \approx \left| 1 - \sum_{i=1}^{N_4} \sum_{j=1}^{N_4} \bar{f}_c([\hat{u}_i, \hat{v}_j], \theta) \Delta^2 \right|, \quad (9)$$

### 3) Non-negativity Constraint for Neural Copula

The PDF of all points on the domain of the Copula function should be non-negative. In the training process, we need to punish the case where PDF is negative. When PDF is continuous, the non-negativity loss can be formulated as:

$$L^N(\theta) = \int_{u_i \in \mathbf{u}} \int_{v_j \in \mathbf{v}} \text{ReLU}(-f_c([u_i, v_j], \theta)) du_i dv_j, \quad (10)$$



Then, we need to leverage the same idea of the formula (9) to approximate the formula (10). Suppose that  $\dot{\mathbf{u}} = [\dot{u}_1, \dot{u}_2, \dots, \dot{u}_{N_5}]$  and  $\dot{\mathbf{v}} = [\dot{v}_1, \dot{v}_2, \dots, \dot{v}_{N_5}]$  are two linearly spaced vectors with  $N_5$  points generated between 0 and 1. The non-negativity loss can be re-written as:

$$L^N(\boldsymbol{\theta}) \approx \frac{1}{(N_5)^2} \sum_{i=1}^{N_5} \sum_{j=1}^{N_5} \text{ReLU}(-f_c([\dot{u}_i, \dot{v}_j], \boldsymbol{\theta})), \quad (11)$$

#### 4) Maximum Likelihood Estimation for Neural Copula

The fitness of the neural Copula model to the data  $\tilde{\mathbf{u}}$  and  $\tilde{\mathbf{v}}$  (acquired from  $\Gamma^{T_1}$  and  $\Gamma^{T_2}$  in the formula(4)) is implemented by the idea of maximum likelihood (ML) estimation. The loss for maximum likelihood estimation can be formally expressed as:

$$L^M(\boldsymbol{\theta}) = \frac{1}{N_2} \left| \eta - \sum_{i=1}^{N_2} \log(\bar{f}_c([\tilde{u}_i, \tilde{v}_i], \boldsymbol{\theta})) \right|, \quad (12)$$

Theoretically, the  $\eta$  should be a positive infinite value. In our experiments, we empirically find that setting  $\eta$  to 10 is sufficient.

#### 5) Observation Constraint for Neural Copula

To ensure the consistency between the CDF of the neural Copula and the empirical CDF of the original data, we need to sample certain observation points to narrow the generated CDF and the empirical CDF at these points. Suppose that  $\mathbf{x} = [x_1, x_2, \dots, x_{N_6}]$  and  $\mathbf{y} = [y_1, y_2, \dots, y_{N_6}]$  are two linearly spaced vectors with  $N_6$  observation points generated between 0 and 1. The CDF values of  $\mathbf{x}$  and  $\mathbf{y}$  generated from the distribution of  $\Gamma^{T_1}$  and  $\Gamma^{T_2}$  are  $\bar{\mathbf{u}}$  and  $\bar{\mathbf{v}}$ , respectively. The observation loss can be written as:

$$L^O(\boldsymbol{\theta}) = \sum_{i=1}^{N_6} \sum_{j=1}^{N_6} \left| \tilde{C}(\bar{u}_i, \bar{v}_j, \boldsymbol{\theta}_c) - \frac{\sum_{m=1}^{N_2} I(\gamma_m^{T_1} \leq x_i, \gamma_m^{T_2} \leq y_j)}{N_2} \right|, \quad (13)$$

where  $I(\cdot)$  is the indicator function as follows:

$$I(z) = \begin{cases} 1 & \text{if } z \\ 0 & \text{if not } z \end{cases}, \quad (14)$$

Finally, we linearly combine the above five constraint loss using certain weights. Formally,

$$L(\boldsymbol{\theta}) = w_B L^B(\boldsymbol{\theta}) + w_I L^I(\boldsymbol{\theta}) + w_N L^N(\boldsymbol{\theta}) + w_M L^M(\boldsymbol{\theta}) + w_O L^O(\boldsymbol{\theta}), \quad (15)$$

In our experiment, we set the weights  $[w_B, w_I, w_N, w_M, w_O]$  equaling to  $[2, 0.3, 1, 0.1, 5]$  that is empirically found to be robust for most cases.

#### D. Model Inference for CD Result

After the training of the neural Copula model is over, we can exploit the trained neural Copula model to infer the changes between  $I^{T_1}$  and  $I^{T_2}$ . The process of CD inference is composed of four steps: superpixel segmentation, feature extraction, neural Copula model inferring, and clustering segmentation.

The first step of model inference is superpixel segmentation. We use the same superpixel segmentation algorithm from [28] in Section III-B to cut the original image pairs into certain image patch pairs. Formally,

$$\begin{aligned}\Phi^{T_1}, \Phi^{T_2} &= \overline{SLIC}(I^{T_1}, I^{T_2}, N_7), \\ \Phi^{T_1} &= \{\Phi_i^{T_1} | i = 1, 2, \dots, N_7\}, \\ \Phi^{T_2} &= \{\Phi_i^{T_2} | i = 1, 2, \dots, N_7\},\end{aligned}\tag{16}$$

where  $\Phi^{T_1}$  and  $\Phi^{T_2}$  are segmentation sets of  $I^{T_1}$  and  $I^{T_2}$  with  $N_7$  superpixels, respectively.  $\Phi_i^{T_1}$  and  $\Phi_i^{T_2}$  are the  $i$ -th superpixel in  $\Phi^{T_1}$  and  $\Phi^{T_2}$ , respectively.

Then, we extract the feature of each superpixel in  $\Phi^{T_1}$  and  $\Phi^{T_2}$ . Same as Section III-C, we choose the average value of all pixels in one superpixel as the feature value representing the superpixel. Formally,

$$\begin{aligned}Z^{T_1} &= \{z_i^{T_1} = \text{Floor}(\text{Mean}(\Phi_i^{T_1})), 1 \leq i \leq N_7\}, \\ Z^{T_2} &= \{z_i^{T_2} = \text{Floor}(\text{Mean}(\Phi_i^{T_2})), 1 \leq i \leq N_7\},\end{aligned}\tag{17}$$

The next step is to transform  $Z^{T_1}$  and  $Z^{T_2}$  into probability space, i.e., estimating the CDF values for every point in  $Z^{T_1}$  and  $Z^{T_2}$ . To keep the CDF estimation consistent for the marginal distributions during the training and testing process, we estimate the CDF values at every point in  $Z^{T_1}$  and  $Z^{T_2}$  according to the marginal distribution fitted by the training sets  $\Gamma^{T_1}$  and  $\Gamma^{T_2}$ , respectively. Formally,

$$\begin{aligned}\ddot{\mathbf{u}} &= KDE(\Gamma^{T_1}, Z^{T_1}) \\ \ddot{\mathbf{v}} &= KDE(\Gamma^{T_2}, Z^{T_2}),\end{aligned}\tag{18}$$

where  $\ddot{\mathbf{u}} \in \mathbb{R}^{N_7 \times 1}$  and  $\ddot{\mathbf{v}} \in \mathbb{R}^{N_7 \times 1}$  are the CDF values of  $Z^{T_1}$  and  $Z^{T_2}$ , respectively. Afterward, we input the  $\ddot{\mathbf{u}}$  and  $\ddot{\mathbf{v}}$  into the trained Copula model and calculate the PDF values of the neural Copula model via differentiation as the formula (5):

$$\bar{f}_{\tilde{C}}([\ddot{\mathbf{u}}, \ddot{\mathbf{v}}], \boldsymbol{\theta}) = ReLU\left(\frac{\tilde{C}([\ddot{\mathbf{u}}, \ddot{\mathbf{v}}], \boldsymbol{\theta})}{\partial \ddot{\mathbf{u}} \partial \ddot{\mathbf{v}}}\right) + \rho,\tag{19}$$

where  $\bar{f}_{\tilde{C}}([\ddot{\mathbf{u}}, \ddot{\mathbf{v}}], \boldsymbol{\theta}) \in \mathbb{R}^{N_7 \times 1}$  represents the unchanged correlation coefficient of  $N_7$

superpixel pairs in a point-to-point form. Then, we normalize the correlation coefficient  $\bar{f}_{\hat{C}}([\tilde{\mathbf{u}}, \tilde{\mathbf{v}}], \boldsymbol{\theta})$  via negative logarithmic operation. Afterward, we use the fuzzy c-means clustering algorithm [31] to divide  $-\log_{10}(f_{\hat{C}}([\tilde{\mathbf{u}}, \tilde{\mathbf{v}}], \boldsymbol{\theta}))$  into two categories, i.e., classifying the superpixels into the changed and unchanged regions. Finally, we can obtain the CD results by assigning the categories of the superpixels to the corresponding pixels.

## IV. Experiment Results

In this section, we evaluate the validity of the proposed NN-Copula-CD algorithm on three heterogeneous datasets and compare it with several state-of-the-art (SOTA) heterogeneous CD methods. In addition, we conduct in-depth discussion to explore the factors affecting the performance of the NN-Copula-CD algorithm.

### A. Dataset

The first dataset from [14] indicates a flood in Gloucester, England, as shown in Fig. 3. It consists of a pre-change SAR (Synthetic Aperture Radar) image shot by ERS satellite on Oct. 21, 1999, and a post-change NDVI (Normalized Difference Vegetation Index) image acquired in 2000. We follow the same preprocessing operation in [14] and the size of the heterogeneous image pair is  $2359 \times 1318$ .

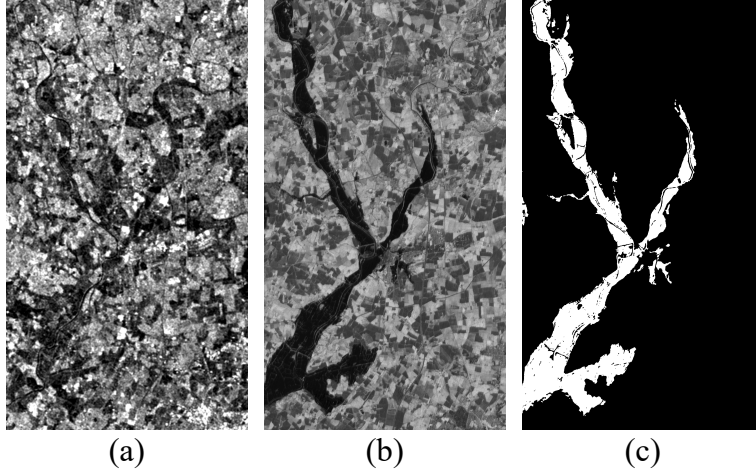


Fig. 3. The first dataset of the flood in Gloucester, England. (a) The pre-change SAR image was acquired in 1999. (b) The post-change NDVI image was acquired in 2000. (c) Ground truth. The size of the two images in this dataset is  $2359 \times 1318$ .

The second dataset displayed in Fig. 4 is a flood that occurs in Wujiabao town, China. This dataset contains a pre-change SAR image shot by the Sentinel-1 satellite on Sep. 20, 2021,

and a post-change NIR (Near Infra-Red) image shot by the Sentinel-2 satellite on Oct. 16, 2021. The ground truth is provided by the Tsinghua university. The size of the two images in this dataset is  $1024 \times 1024$ .

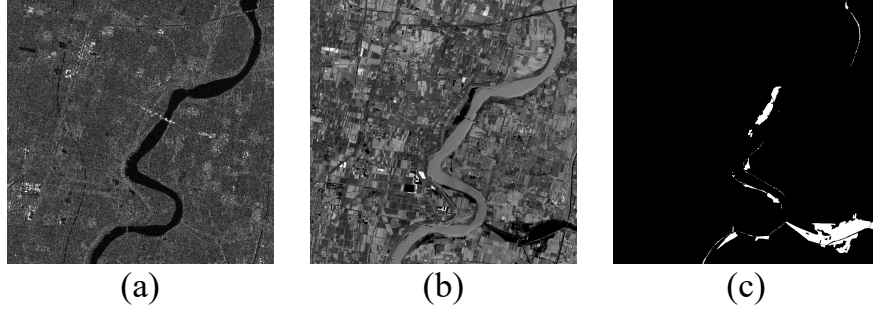


Fig. 4. The second dataset of the flood in Wujiabao town, China. (a) The pre-change SAR image was acquired on Sep. 20, 2021. (b) The post-change NIR image was acquired on Oct. 16, 2021. (c) Ground truth. The size of the two images in this dataset is  $1024 \times 1024$ .

The third dataset shown in Fig. 5 is provided by [32] and it reflects the urban construction in Toulouse, Fr from 2009 to 2013. This dataset is composed of a pre-change SAR image shot by the TerraSAR-X satellite in 2009 and a post-change optical image shot by the Pleiades satellite in 2013. The optical image is originally provided in grayscale form with a size of  $4404 \times 2600$  while the size of the SAR image is  $4404 \times 2604$ . Thus, we crop the SAR image into the size of  $4404 \times 2600$  same as the optical image.

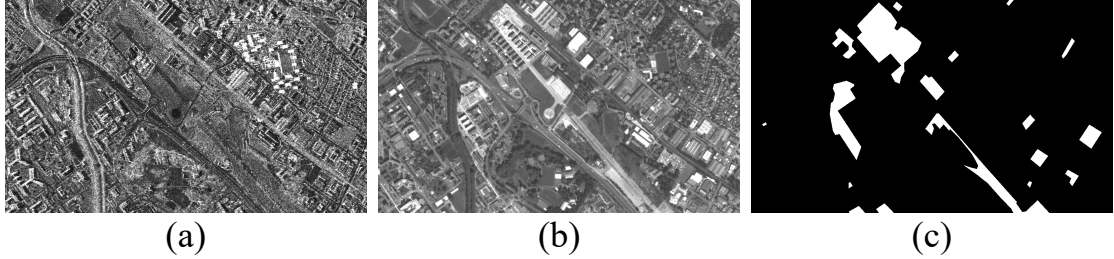


Fig. 5. The third dataset of the construction in Toulouse, Fr. (a) The pre-change SAR image acquired in 2009. (b) The post-change optical image was acquired in 2013. (c) Ground truth. The size of the two images in this dataset is  $4404 \times 2600$ .

## B. Experiment Setting

### 1) The SOTA Competitors of heterogeneous CD

In our experiments, we compare the proposed NN-Copula-CD method with several representative SOTA methods for heterogeneous CD, i.e., HPT[12], SCCN[14], and M3CD [32].

HPT [12] is a semi-supervised method based on homogeneous pixel transformation. It aligns the pixel-level features of two images in a homogeneous space by transforming the feature of one image into the feature space of the other image. Then, the CD result is convenient to produce by feature difference and clustering algorithm. During the training process, some well-chosen unchanged regions are treated as the training samples to ensure robustness under the interference of heterogeneity and noise.

SCCN [14] is an unsupervised method based on a deep convolutional coupling network. It first exploits two denoising autoencoders (DAE) to initialize each side of the network. Then it trains the two sides of the network collaboratively to transform the two images in the same feature space. Finally, it obtains the CD results by classifying the difference map of two sides of the network via a thresholding algorithm.

M3CD [32] is an unsupervised method based on a pixel pair-based Markovian model. The M3CD method first builds a Markovian mixture model with well-estimated parameters and then optimizes the Maximum a posteriori (MAP) problem to calculate the CD results.

### 2) Evaluation measurements

we adopt four measurements, i.e., the numbers of false positive (FP), false negative (FN) predictions, percentage correct classification (PCC), and Kappa coefficient (KC) to evaluate the performance of the proposed NN-Copula-CD method and the competitors. The definition of the PCC and Kappa is followed as:

$$\begin{aligned} OE &= (TP + TN) / (TP + TN + FN + FP), \\ PCC &= (TP + TN) / (TP + TN + FN + FP), \\ F1 &= \frac{(TP + FN)(TP + FP) + (TN + FP)(TN + FN)}{(TP + TN + FP + FN)^2}, \\ KC &= (PCC - PRE) / (1 - PRE), \end{aligned} \quad (20)$$

where TP and TN are the numbers of true positive and true negative predictions, respectively. Note that higher PCC reflects better detection accuracy of the method while higher KC indicates the better comprehensive performance of the method.

### 3) Implementation details

Our NN-Copula-CD method is implemented by the Keras framework. We train the NN-Copula model on one NVIDIA RTX TITAN GPU. In fact, the computational burden needed to train the NN-Copula model is very small since it is just a fully connected neural network with five hidden layers. In the training process, we use the Nesterov Adam optimizer to

optimize the NN-Copula model and the learning rate is set to 0.001. The total training epochs are set to 25000. When the training process is over, we chose the model with the least loss  $L(\theta)$  as the inference model to produce the CD results. The  $N_1$  and  $N_2$  representing the num of superpixels are set to 6000 and 3000 respectively for the first and second datasets while 8000 and 3000 respectively for the third dataset. The reason for the difference in the third dataset is that the size of the third dataset is much larger than the first and second datasets. The  $N_3$  representing the num of the simulated points on the boundary of Copula function is set to 400. The  $N_4$  and  $N_5$  representing the num of the simulated points in Copula function are both set to 256. The  $N_6$  representing number of observation points is set to 100.

### C. Performance Comparison

The quantitative performance and the visualization results of different methods on three datasets are reported in Table I and Fig. 6, respectively. In our experiment, we exploit the same selected unchanged samples to train the semi-supervised methods including HPT [12] and our method, as shown in Fig. 6(a). From the quantitative comparison in Table I, we can find that the proposed NN-Copula-CD algorithm achieves the highest score of KC (i.e., the synthetical evaluation indicator) on three datasets. Besides, our model obtains the highest score of PCC on the first dataset while the second-highest score of PCC on the second and third datasets. The semi-supervised competitor HPT [12] achieves the second-best performance on the flood detection of the first and second datasets, yet it exhibits poor adaptability to the third dataset. The reason for this is that the heterogeneity in city scenes is much more complex than the flood scenes (especially for SAR images containing many buildings with metallic reflection), and the homogeneous pixel transformation in [12] suffers from the limited transformation capabilities to align two images into the same feature space. The unsupervised DNN-based SCCN [14] achieves an improved performance than HPT [12] on the third dataset, yet SCCN [14] still struggles to converge stably and detect robustly due to the lack of interpretability for its deep convolutional layers. Compared to the SOTA competitors, the proposed NN-Copula-CD significantly reduces the FN predictions where the changed areas identified by the proposed NN-Copula-CD are more complete.

TABLE I

Comparison results of different methods on the three datasets. PCC and KC are written in (%). The

highest score is marked in bold. The second-best score is marked in underlined.

	The First Dataset FP / FN / OE / PCC / KC	The Second Dataset FP / FN / OE / PCC / KC	The Third Dataset FP / FN / OE / PCC / KC
M3CD	94173 / 186156 / 280329 / 90.98 / 51.81	67285 / 10782 / 78067 / 92.55 / 25.88	<b>403308</b> / 620994 / <b>1024302</b> / <b>91.07</b> / <u>31.6</u>
SCCN	<b>205</b> / 160623 / 160828 / 94.83 / 69.63	<b>19246</b> / 11728 / <b>30974</b> / <b>97.05</b> / 47.34	3623648 / <b>251655</b> / 3875303 / 66.16 / 14.09
HPT	<u>26289</u> / <u>114837</u> / <u>141126</u> / <u>95.46</u> / <u>75.85</u>	33890 / <u>5554</u> / 39444 / 96.24 / <u>49.81</u>	<u>1250195</u> / 749325 / 1999520 / 82.54 / 4.61
NN-Copula-CD	65972 / <b>37711</b> / <b>103683</b> / <b>96.67</b> / <b>84.60</b>	<u>26672</u> / <b>5026</b> / <u>31698</u> / <u>96.98</u> / <b>56.12</b>	1393486 / <u>325175</u> / <u>1718661</u> / <u>84.99</u> / <b>33.22</b>

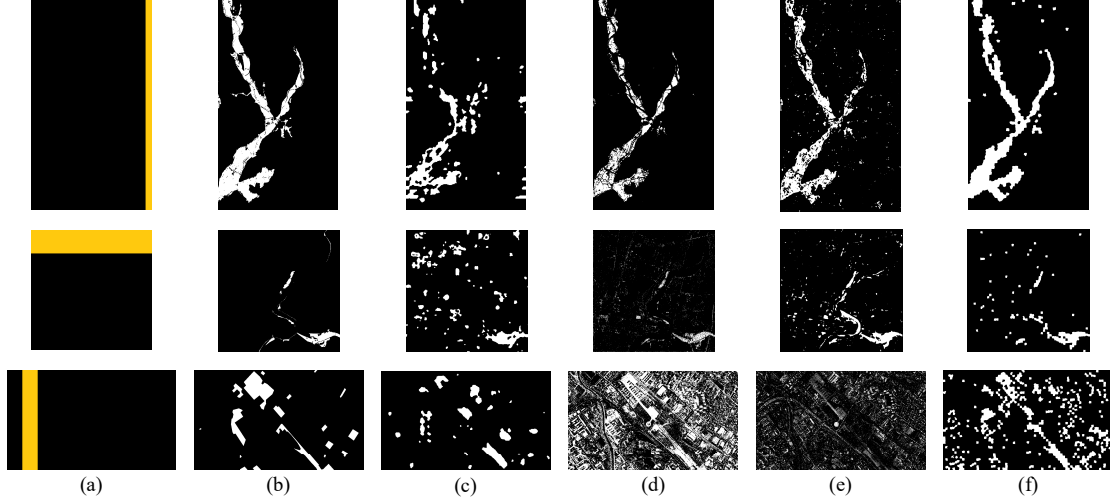


Fig. 6. The visualized CD results of different methods on three datasets. (a) The selected region (marked by orange) is used to train the semi-supervised methods including HPT [9] and our NN-Copula-CD. (b) Ground Truth. (c) M3CD [32]. (d) SCCN [14]. (e) HPT [12]. (f) The proposed NN-Copula-CD.

TABLE II

Comparison results between traditional Copulas and neural Copula on the three datasets. PCC and KC are written in (%). The highest score is marked in bold.

	The First Dataset FP / FN / OE / PCC / KC	The Second Dataset FP / FN / OE / PCC / KC	The Third Dataset FP / FN / OE / PCC / KC
Gaussian Copula	21368 / 151742 / 173110 / 94.43 / 68.67	265990 / 12739 / 278729 / 73.42 / 4.59	3322561 / 579027 / 3901588 / 65.93 / 2.03
Student T Copula	32524 / 122226 / 154750 / 95.02 / 73.48	281110 / 12967 / 294077 / 71.95 / 3.98	1531736 / 355319 / 1887055 / 83.52 / 29.18
Clayton Copula	<b>7642</b> / 232313 / 239955 / 92.28 / 50.07	72179 / 8579 / 80758 / 92.30 / 27.94	7918545 / <b>127543</b> / 8046088 / 29.73 / 2.21
Frank Copula	181822 / 111006 / 292828 / 90.58 / 58.51	384116 / 8728 / 392844 / 62.54 / 3.74	4528153 / 404975 / 4933128 / 56.92 / 4.08
Neural Copula	65972 / <b>37711</b> / <b>103683</b> / <b>96.67</b> / <b>84.60</b>	<u>26672</u> / <b>5026</b> / <u>31698</u> / <u>96.98</u> / <b>56.12</b>	<b>1393486</b> / 325175 / <b>1718661</b> / <u>84.99</u> / <b>33.22</b>

To more intuitively understand the interpretability and the effectiveness of our NN-Copula-CD algorithm, we display the empirical joint distribution of the original training samples (i.e.,  $\Gamma^{T_1}$  and  $\Gamma^{T_2}$ ) and the joint distribution learned by the Neural Copula in Fig 7. It can be observed that our NN-Copula-CD effectively learns the correlation between bi-temporal heterogeneous images via the guidance of Copula theory, which facilitates the neural network to understand complex change patterns from the perspective of probability space. Compared

to the other deep-neural-network-based methods [14], our network has a simple structure with high theoretical interpretability, which facilitates us to better exploit the potential of network parameters instead of stacking more deep neural layers.

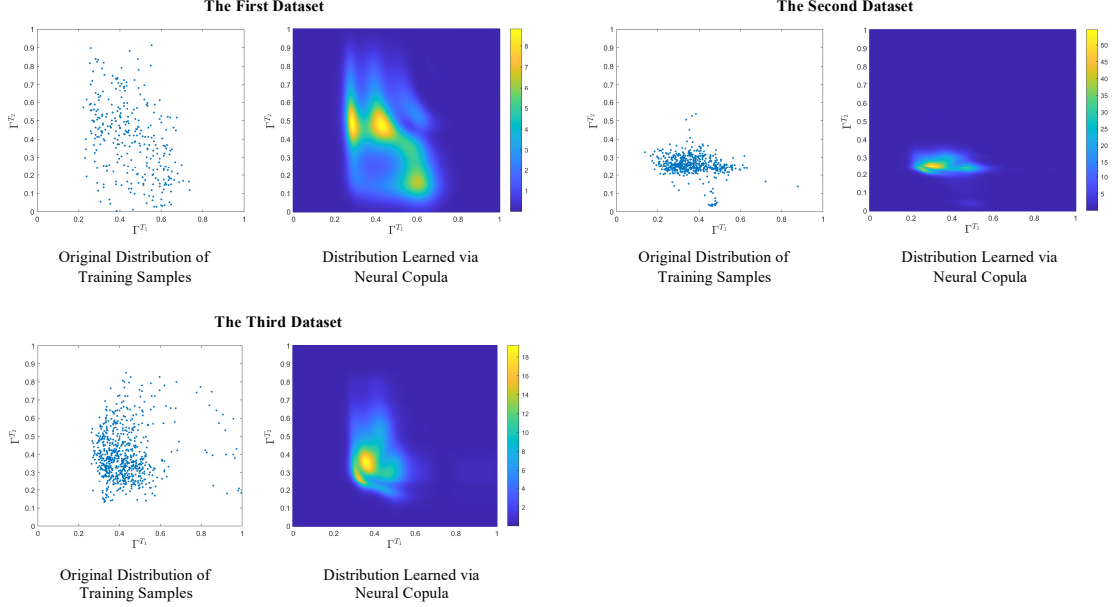


Fig. 7. The empirical joint distribution of the original training samples (i.e.,  $\Gamma^{T_1}$  and  $\Gamma^{T_2}$ ) and the simulated joint distribution learned by the Neural Copula.

#### D. Discussion

**Discussion on the effectiveness comparison between traditional Copula functions and the neural Copula model.** To demonstrate the superiority of the neural Copula compared to the traditional Copula functions, we replace the neural Copula model with several typical traditional Copula functions, i.e., student T Copula, gaussian Copula, Clayton Copula, and frank Copula. The quantitative results in Table II and the visualized results in Fig. 8 show that the neural Copula surpasses the traditional Copulas on three datasets. This is because the neural Copula model is both knowledge-driven and data-driven, and it can learn the complex correlation flexibly from heterogeneous remote sensing data while keeping sufficient interpretability at theoretical level.



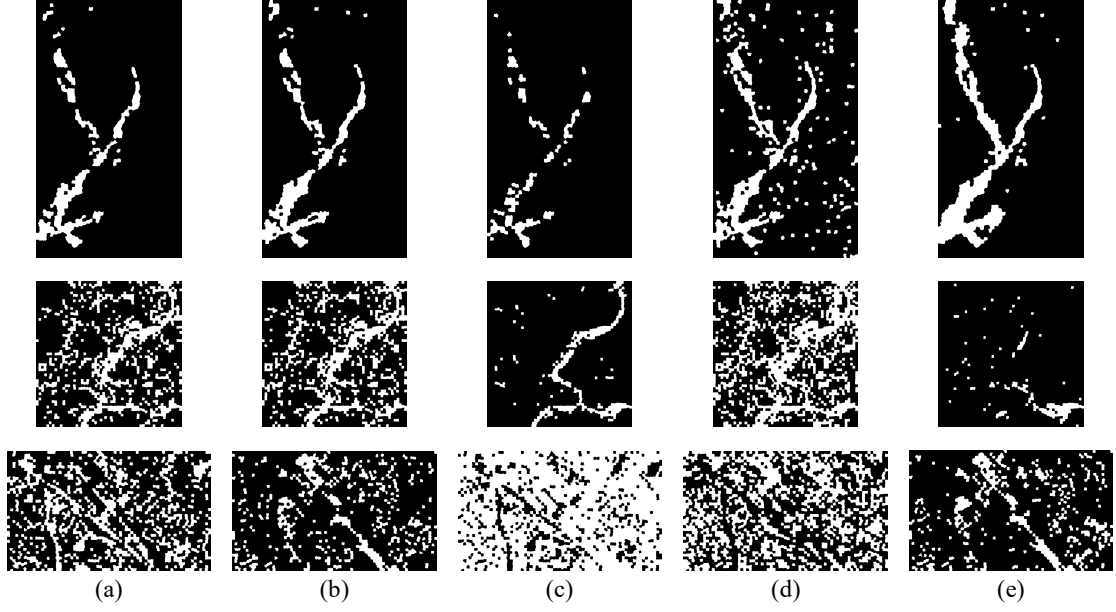


Fig. 8. The CD results of the traditional Copulas and neural Copula on three datasets. (a) Gaussian Copula. (b) Student T Copula. (c) Clayton Copula. (d) Frank Copula. (e) Neural Copula.

For a more intuitive comparison between the neural Copula and traditional Copulas, we visualize the joint distribution of  $I^{T_1}$  and  $I^{T_2}$  fitted by neural Copula and traditional Copulas in the first dataset, respectively. In Fig. 9, we can observe that the traditional Copulas fit the data with the regular forms and have the under-fitting problems due to their fixed mathematical expressions. Compared to the traditional Copulas, the neural Copula has more flexibility that facilitates it to learn the distribution in a more detailed manner. Therefore, it is more competent than traditional Copula to fit the complex correlation between heterogeneous remote sensing data.

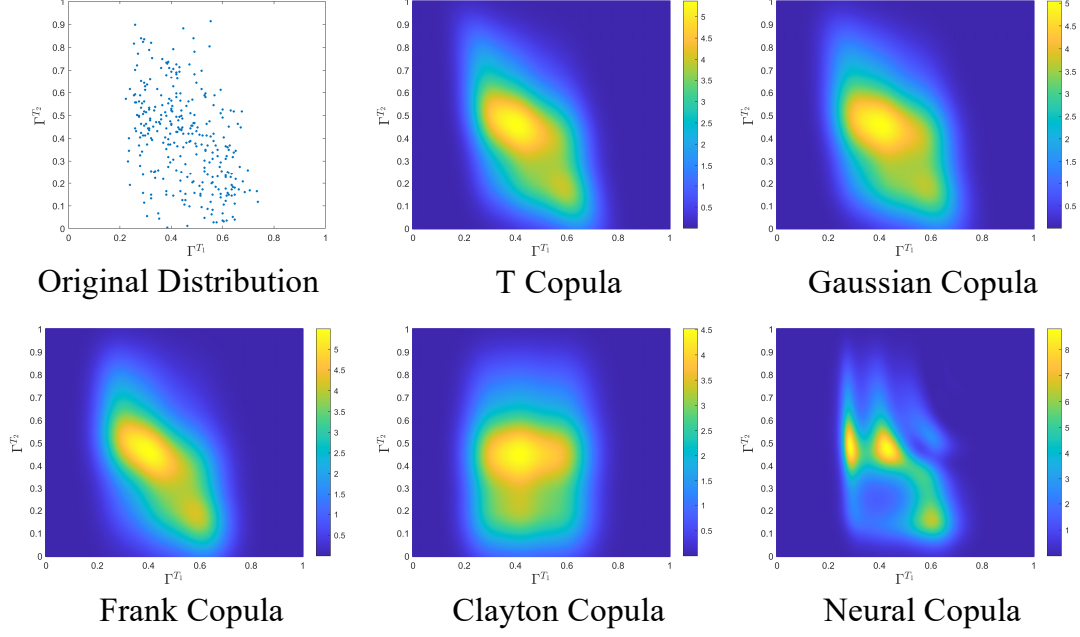


Fig. 9. The joint distribution of  $\Gamma^{T_1}$  and  $\Gamma^{T_2}$  fitted by neural Copula and traditional Copulas at the first dataset, respectively.

**Discussion on the number of selected training samples.** To investigate the influence of difference of training samples on the performance of the NN-Copula-CD algorithm, we conduct the ablation experiments in the first dataset. We cut the three image patch pairs containing 5.3%, 9.8%, and 16.6% pixels respectively from the original image pairs to train the neural Copula model with other settings fixed. The quantitative results using different proportions of training samples are shown in Table III.

TABLE III  
Quantitative Evaluation for Different Proportion of Training Samples. PCC and KC are written in (%).

Proportion of Training Samples	FP	FN	OE	PCC	KC
5.31%	65972	37711	103683	96.67	84.60
9.86%	62436	52426	114862	96.31	82.58
16.61%	68944	60110	129054	95.85	80.40

The training samples that are chosen to train the network and the visualization results corresponding to different proportions of training samples are displayed in Fig. 10. We can observe that the performance of the NN-Copula-CD method achieves the highest KC of 84.6% using 5.3% training samples. With more training samples, the performance of the NN-Copula-

CD method doesn't show an expected growth. We speculate that two possible reasons lead to this phenomenon: The first reason is that more samples bring higher modeling challenges, and the fixed model capacity cannot adapt to the growing complexity of the samples. The second reason is that we directly segment a regular region in original images as the training samples. Compare to those well-chosen training samples with high quality in HPT [12], the training samples chosen by us are not elaborate enough. Although our treatment of training samples is time-efficient and labor-saving, it may bring more noise and unbalanced samples that influences the performance of the methods.

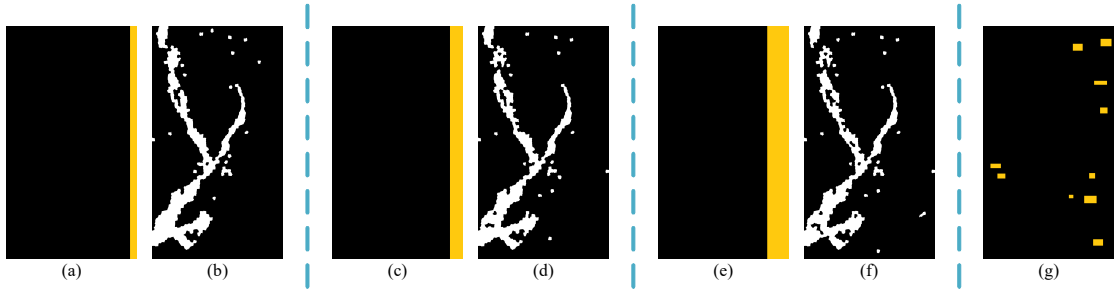


Fig. 10. The CD results using different proportions of training samples. The selected training samples are represented in orange color. (a) The training samples with 5.31% pixels. (b) The CD result of our method using 5.31% training samples. (c) The training samples with 9.86% pixels. (d) The CD result of our method with 9.86% training samples. (e) The training samples with 16.61% pixels. (f) The CD result of our method using 16.61% training samples. (g) The well-chosen samples in the paper of HPT [12].

**Discussion on the number of trainable parameters in the neural Copula model.** To analyze how the number of trainable parameters in the neural Copula model influences the CD performance, we design three versions of the neural Copula models, i.e., the tiny version with 481 parameters, the medium version with 1021 parameters, and the large version with 1761 parameters. The tiny, middle, and large models all contain five hidden layers with 10, 15, and 20 neurons, respectively. Then, we fix other experiment settings and test the three versions of the neural Copula models with 5.3% training samples on the first dataset. As the quantitative comparison shown in Table IV, the middle version surpasses the other two versions on both PCC and KC. We visualize the training process of three versions in Fig. 11. Compared with the middle version, the tiny version exhibits an under-fitting trend, and the large version converges fast but shows limited generalization due to the overfitting to the empirical distribution of the original data.

TABLE IV

Quantitative Evaluation for Different Parameters of the Neural Copula Model. PCC and KC are written in (%).

Model Size	FP	FN	OE	PCC	KC
Tiny (481 Params)	56015	53398	109413	96.48	83.27
Middle (1021 Params)	64656	37197	101853	96.72	84.86
Large (1761 Params)	65972	37711	103683	96.67	84.60

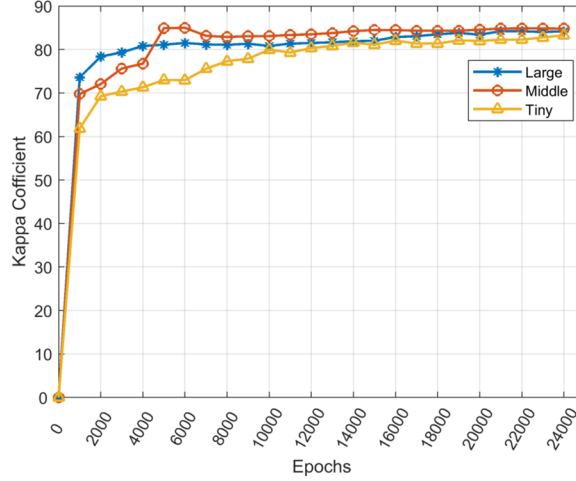


Fig. 11. The training process of neural Copula models of different sizes.

## V. Conclusion

In this paper, we propose a novel semi-supervised method based on the Copula-guided neural network, named NN-Copula-CD, to address the CD problem in heterogeneous remote sensing images. In the proposed NN-Copula-CD, we transform CD into a correlation measurement issue where the changes can be efficiently identified via comparison of the correlations of remote sensing region pairs in the probability space. Different from the most existing DNN-based heterogeneous CD methods that depend on the powerful representation capabilities of DNNs without sufficient trustworthiness and controllability, the proposed NN-Copula-CD can exploit a simple fully connected network that is interpretable via Copula theory to achieve a similar or even better CD performance than DNNs, which further confirms the benefits of interpretability that facilitates the efficiency of neural network for heterogeneous CD. Besides, the NN-Copula-CD further extends the robustness and usability of the traditional Copula functions for heterogeneous remote sensing data. The in-depth experiments on three CD datasets with multi-modal remote sensing images demonstrate the

effectiveness and interpretability of our NN-Copula-CD. Furthermore, the visualized results intuitively explain the superiority and interpretability compared to the existing DNN-based and the traditional Copula-based heterogeneous CD methods. In the future, we will further investigate the improvement of the NN-Copula-CD method on heterogeneous CD problem.

## VI. Reference

- [1] X. Jiang, G. Li, X.-P. Zhang, and Y. He, "A semisupervised siamese network for efficient change detection in heterogeneous remote sensing images," *IEEE Transactions on Geoscience and Remote Sensing*, vol. 60, pp. 1-18, 2021.
- [2] Z. Zheng, Y. Zhong, J. Wang, A. Ma, and L. Zhang, "Building damage assessment for rapid disaster response with a deep object-based semantic change detection framework: From natural disasters to man-made disasters," *Remote Sensing of Environment*, vol. 265, pp. 112636, 2021.
- [3] M. K. Ridd, and J. Liu, "A comparison of four algorithms for change detection in an urban environment," *Remote sensing of environment*, vol. 63, no. 2, pp. 95-100, 1998.
- [4] S. H. Khan, X. He, F. Porikli, and M. Bennamoun, "Forest change detection in incomplete satellite images with deep neural networks," *IEEE Transactions on Geoscience and Remote Sensing*, vol. 55, no. 9, pp. 5407-5423, 2017.
- [5] R. D. Jackson, "Spectral indices in N-Space," *Remote Sensing of Environment*, vol. 13, no. 5, pp. 409-421, 1983/11/01/, 1983.
- [6] W. J. Todd, "Urban and regional land use change detected by using Landsat data," *Journal of Research of the U.S. Geological Survey*, vol. 5, no. 5, pp. 529-534, 1977.
- [7] P. J. Howarth, and G. M. Wickware, "Procedures for change detection using Landsat digital data," *International Journal of Remote Sensing*, vol. 2, no. 3, pp. 277-291, 1981/07/01, 1981.
- [8] L. Wan, Y. Xiang, and H. You, "A Post-Classification Comparison Method for SAR and Optical Images Change Detection," *IEEE Geoscience and Remote Sensing Letters*, vol. 16, no. 7, pp. 1026-1030, 2019.
- [9] L. Wan, Y. Xiang, and H. You, "An Object-Based Hierarchical Compound Classification Method for Change Detection in Heterogeneous Optical and SAR Images," *IEEE Transactions on Geoscience and Remote Sensing*, vol. 57, no. 12, pp. 9941-9959, 2019.
- [10] D. Brunner, L. Bruzzone, and G. Lemoine, "Change detection for earthquake damage assessment in built-up areas using very high resolution optical and SAR imagery." pp. 3210-3213.
- [11] D. Brunner, G. Lemoine, and L. Bruzzone, "Earthquake Damage Assessment of Buildings Using VHR Optical and SAR Imagery," *IEEE Transactions on Geoscience and Remote Sensing*, vol. 48, no. 5, pp. 2403-2420, 2010.
- [12] Z. Liu, G. Li, G. Mercier, Y. He, and Q. Pan, "Change detection in heterogeneous remote sensing images via homogeneous pixel transformation," *IEEE Transactions on*

*Image Processing*, vol. 27, no. 4, pp. 1822-1834, 2018.

- [13] Z.-g. Liu, L. Zhang, G. Li, and Y. He, "Change detection in heterogeneous remote sensing images based on the fusion of pixel transformation." pp. 1-6.
- [14] J. Liu, M. Gong, K. Qin, and P. Zhang, "A deep convolutional coupling network for change detection based on heterogeneous optical and radar images," *IEEE transactions on neural networks and learning systems*, vol. 29, no. 3, pp. 545-559, 2016.
- [15] X. Jiang, G. Li, Y. Liu, X.-P. Zhang, and Y. He, "Homogeneous transformation based on deep-level features in heterogeneous remote sensing images." pp. 206-209.
- [16] X. Jiang, G. Li, Y. Liu, X.-P. Zhang, and Y. He, "Change detection in heterogeneous optical and SAR remote sensing images via deep homogeneous feature fusion," *IEEE Journal of Selected Topics in Applied Earth Observations and Remote Sensing*, vol. 13, pp. 1551-1566, 2020.
- [17] X. Li, Z. Du, Y. Huang, and Z. Tan, "A deep translation (GAN) based change detection network for optical and SAR remote sensing images," *ISPRS Journal of Photogrammetry and Remote Sensing*, vol. 179, pp. 14-34, 2021.
- [18] Z.-G. Liu, Z.-W. Zhang, Q. Pan, and L.-B. Ning, "Unsupervised change detection from heterogeneous data based on image translation," *IEEE Transactions on Geoscience and Remote Sensing*, vol. 60, pp. 1-13, 2021.
- [19] X. Niu, M. Gong, T. Zhan, and Y. Yang, "A conditional adversarial network for change detection in heterogeneous images," *IEEE Geoscience and Remote Sensing Letters*, vol. 16, no. 1, pp. 45-49, 2018.
- [20] L. T. Luppino, M. Kampffmeyer, F. M. Bianchi, G. Moser, S. B. Serpico, R. Jenssen, and S. N. Anfinsen, "Deep image translation with an affinity-based change prior for unsupervised multimodal change detection," *IEEE Transactions on Geoscience and Remote Sensing*, vol. 60, pp. 1-22, 2021.
- [21] L. T. Luppino, M. A. Hansen, M. Kampffmeyer, F. M. Bianchi, G. Moser, R. Jenssen, and S. N. Anfinsen, "Code-aligned autoencoders for unsupervised change detection in multimodal remote sensing images," *IEEE Transactions on Neural Networks and Learning Systems*, 2022.
- [22] G. Mercier, G. Moser, and S. Serpico, "Conditional copula for change detection on heterogeneous SAR data." pp. 2394-2397.
- [23] G. Mercier, G. Moser, and S. B. Serpico, "Conditional Copulas for Change Detection in Heterogeneous Remote Sensing Images," *IEEE Transactions on Geoscience and Remote Sensing*, vol. 46, no. 5, pp. 1428-1441, 2008.
- [24] Z. Zeng, and T. Wang, "Neural Copula: A unified framework for estimating generic high-dimensional Copula functions," *arXiv preprint arXiv:2205.15031*, 2022.
- [25] T. Janke, M. Ghanmi, and F. Steinke, "Implicit generative copulas," *Advances in Neural Information Processing Systems*, vol. 34, pp. 26028-26039, 2021.
- [26] Y. Ng, A. Hasan, K. Elkhailil, and V. Tarokh, "Generative Archimedean Copulas." pp. 643-653.
- [27] R. Achanta, A. Shaji, K. Smith, A. Lucchi, P. Fua, and S. Ssstrunk, "SLIC superpixels compared to state-of-the-art superpixel methods," *IEEE transactions on pattern analysis and machine intelligence*, vol. 34, no. 11, pp. 2274-2282, 2012.
- [28] Y. Sun, L. Lei, D. Guan, and G. Kuang, "Iterative robust graph for unsupervised

- change detection of heterogeneous remote sensing images,” *IEEE Transactions on Image Processing*, vol. 30, pp. 6277-6291, 2021.
- [29] E. Parzen, “On estimation of a probability density function and mode,” *The annals of mathematical statistics*, vol. 33, no. 3, pp. 1065-1076, 1962.
- [30] A. Krizhevsky, I. Sutskever, and G. E. Hinton, “Imagenet classification with deep convolutional neural networks,” *Communications of the ACM*, vol. 60, no. 6, pp. 84-90, 2017.
- [31] J. C. Bezdek, R. Ehrlich, and W. Full, “FCM: The fuzzy c-means clustering algorithm,” *Computers & geosciences*, vol. 10, no. 2-3, pp. 191-203, 1984.
- [32] R. Touati, M. Mignotte, and M. Dahmane, “Multimodal change detection in remote sensing images using an unsupervised pixel pairwise-based Markov random field model,” *IEEE Transactions on Image Processing*, vol. 29, pp. 757-767, 2019.